Bulletin of the Seismological Society of America, Vol. 96, No. 4A, pp. 1551–1559, August 2006, doi: 10.1785/0120050116

Shear-Wave Structure of the South Indian Lithosphere from Rayleigh Wave Phase-Velocity Measurements

by S. Mitra,* K. Priestley, V. K. Gaur, and S. S. Rai

Abstract We investigate the upper mantle shear-wave speed structure beneath the south Indian shield by measuring and modeling fundamental mode Rayleigh wave phase-velocity dispersion. Observed phase velocities for the south Indian shield closely match those observed for the Canadian shield. We constrain the south Indian crust using published receiver function results and invert the dispersion data for upper mantle shear-wave structure. The ~155-km-thick seismic lithosphere of the south Indian shield is composed of a 35 km-thick, two-layer crust and a ~120-km-thick, high-velocity upper mantle lid. Beneath the Moho the average S_n wave speed is ~4.7 km sec^{-1}. Both S_n travel times data and the dispersion data suggest a positive sub-Moho shear-wave speed gradient. Beneath the seismic lithosphere there is a low-velocity layer where the shear-wave speed drops to ~4.4 km sec^{-1}.

Introduction

Peninsular India is composed of various Precambrian terranes assembled between the mid-Archaean and Neo-Proterozoic. The Dharwar craton together with the Bastar craton accreted to its northwestern edge and granulite terranes to its southern and eastern edges form the south Indian shield. The northwestern part of the shield is overlain by the extensive Cretaceous flood basalts of the Deccan Traps, which thicken progressively toward the northwest. In this study we investigate the upper mantle shear-wave speed structure beneath the south Indian shield by measuring and modeling fundamental mode Rayleigh wave phase-velocity dispersion. There are few previous surface-wave dispersion studies of the upper mantle velocity structure beneath peninsular India. Bhattacharya (1974, 1981) measured Rayleigh wave-group velocity dispersion to about a 100-sec period and from this inferred that the sub-Moho shear-wave speed in the Indian lithosphere was higher than that of the preliminary reference earth model (PREM) and that the upper mantle lid above the low-velocity zone (LVZ) extended to a depth of about 140 km. Hwang and Mitchell (1987) measured Rayleigh wave-phase velocities to 50 sec period but could not detect the base of the high-velocity lid because of the shorter periods of their dispersion data. Our study provides new constraints on the average upper mantle shear-wave speed structure of the south Indian shield by determining two-station, fundamental mode Rayleigh wave-phase velocities for periods up to 200 sec.

*Present address: Department of Geology and Geophysics, Indian Institute of Technology, Kharagpur, India 721 302.

Data and Dispersion Measurements

The data used for this study are broadband seismograms from the National Geophysical Research Institute, Cambridge University, and the Indian Institute of Astrophysics (KOD, NND, BGL, GBA, and LTV), Indian Meteorological Department (BHPL), and Geoscope (HYB) seismographs located on the south Indian shield (Fig. 1). Seismic stations at KOD and NND had Guralp CMG-3T seismometers; BGL, GBA, and LTV had CMG-3ESP seismometers; BHPL had a Streckeisen STS-2 seismometer; and HYB had a Streckeisen STS-1 seismometer. KOD, BHPL, and HYB are permanent sites; NND, BGL, GBA, and LTV were long-term but temporary sites installed within vaults constructed on bedrock. Phase velocities were measured between the various station pairs for three events (Table 1) whose propagation paths deviated by 7° or less from the great-circle arcs connecting the station pairs and the epicenter. We analyzed seismograms from two events in the Himalayan Arc to the north of India and a third event in the Indian Ocean to the south, thereby obtaining a reverse measurement. In addition we used seismograms from several other sites of the Indian Meteorological Department (BLSP, PUNE, and KARD) and the National Geophysical Research Institute (GRR and TPT) to determine the S_n velocity for the south Indian shield (Fig. 2).

We measured phase velocities using the transfer function method of Gomberg *et al.* (1988) in which the phase-velocity determination is posed as a linear filter problem where the seismogram at the far station is expressed as a convolution of the seismogram at the near station with the interstation Earth filter whose determination is sought.

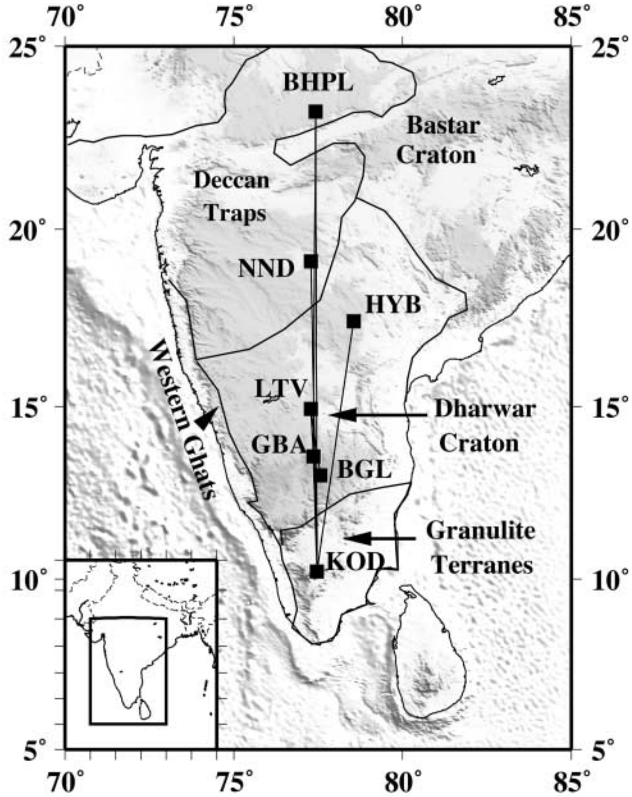

Figure 1. Map of the two station paths for the phase-velocity measurement. The study area is boxed in the key map of India (lower left). The main geologic terranes of the south Indian shield are indicated.

Table 1
Events Used to Determine Long-Period Rayleigh Wave Dispersion

Date (mm/dd/yyyy)	Origin Time	Latitude	Longitude	Depth (km)	M_S
01/24/1999	08 00 08.5	26.463° S	74.476° E	10	6.3
03/28/1999	19 05 11.0	30.512° N	79.403° E	15	6.4
05/12/2000	23 10 30.0	35.970° N	70.660° E	107	6.2

Smoothing constraints were imposed based on an approximate knowledge of the group velocity, and we tested two initial dispersion models and smoothing criteria. The first initial model was derived from the group velocity analysis of Bhattacharya (1981), whereas the second was constructed by placing the average 3SMAC (Nataf and Ricard, 1996) crust between stations onto an upper mantle with a uniform shear-wave velocity of 4.7 km sec^{-1} from the Moho down to 293 km, underlain by a PREM mantle below this depth. The 4.7 km sec^{-1} sub-Moho shear speed used in the second model was based on the data plotted in Figure 2, which shows a composite, reduced-record section formed by 11 seismograms of four Peninsular Indian events recorded by seismographs in southern India. The average S_n wave speed is 4.7 km sec^{-1} but the curvature in the *S*-wave arrival, shown by arrows, suggests that at shallow depths in the mantle lid, the *S*-wave speed is slightly less than 4.7 km sec^{-1} and with a positive velocity gradient throughout the mantle lid. A similar high S_n velocity beneath India was noted by Huest *et al.* (1973).

The final dispersion curve (Fig. 3) was tested for stability in the sense that the resulting dispersion curve was not strongly influenced by realistic perturbations in the initial dispersion model or in the smoothing criteria. The dispersion curve shown in Figure 3 was obtained from the simultaneous inversion of all seismogram pairs, but, to check that there were no large outliers, we also determined dispersion curves for each seismogram pair separately. The errors shown in Figure 3 are estimated statistically from the dispersion calculation and do not reflect systematic errors. The azimuths of the earthquake-propagation paths deviated from the interstation great-circle paths by less than 7°. Because the distance used in calculating the Earth filter is the path difference between the great-circle arcs from the epicenter to each of the stations and not the interstation distance, the main systematic error related to the azimuthal deviation arises from small differences in the initial phase. Priestley and Tilmann (1999) used synthetic seismograms with added noise to estimate the errors arising from the initial phase, as well as the finite-sample interval, and found these to be small.

Figure 3 compares the south India fundamental mode Rayleigh wave phase-velocity dispersion curve with those of some other shields. The Canadian shield phase-velocity curve (Brune and Dorman, 1963) closely matches the dispersion curve for the south Indian shield, whereas that of the south African shield lies close to the south Indian shield curve for periods less than ~40 sec, but is slower for longer periods. On the other hand, the Siberian shield dispersion curve shows the lowest-phase velocities for all periods but approaches that of the south African at about 100 sec. The difference in the phase-velocity curves for the various shield regions most likely reflects differences in the seismic characteristics of their lower crust and upper mantle structures.

Determination of Upper Mantle Structure

Rayleigh wave dispersion is primarily sensitive to shear-wave speeds. We therefore inverted the phase-velocity curve to obtain a shear-wave model for the south Indian shield using the inversion routine of Herrmann (2004). The starting model for the inversion consisted of a two-layer crust of 35-km thickness overlying a CANSD upper mantle velocity structure (Brune and Dorman, 1963). Seismic-controlled source (Kaila and Krishna, 1992) and crustal receiver function analysis (Gupta *et al.*, 2003; Rai *et al.*, 2003) have shown that the crust of the south Indian shield is about 35 km thick and quite uniform over the region of our dispersion measurements. The choice of CANSD as the initial

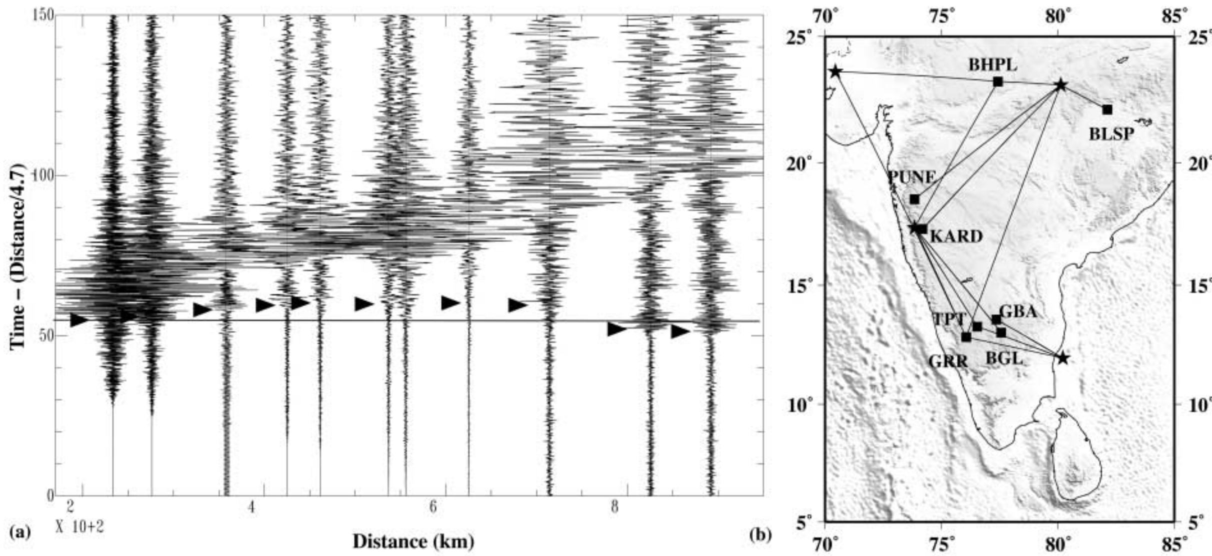

Figure 2. (a) Record section plot of 11 transverse-component seismograms in a distance range of 200–1000 km. The time axis is plotted for a reduction velocity of 4.7 km sec^{-1} (denoted by the horizontal reference line at 55-sec reduced time). The black arrowheads denote the approximate arrival time of the *S* wave. (b) Map showing the earthquake-receiver paths for the data plotted in (a).

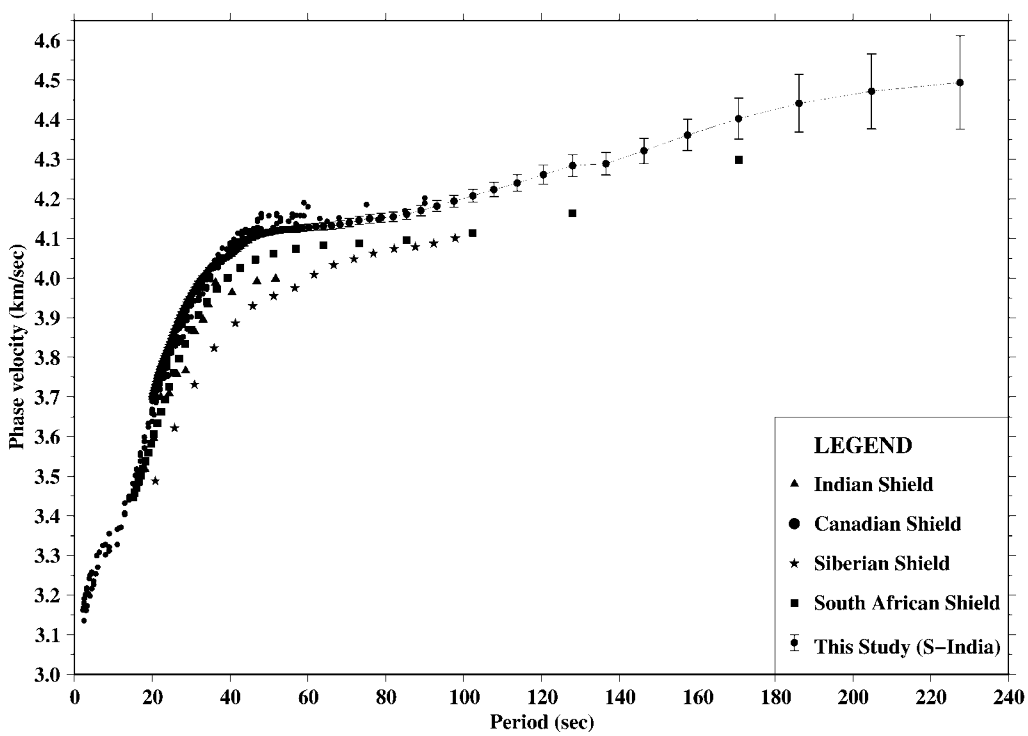

Figure 3. Phase-velocity dispersion curve from this study (labeled S-India), compared with other shield regions. The ±1 S.D. bounds for the phase velocity measured in our study is plotted as vertical bars over the data points. The legend on the plot explains the different symbols used in the plot.

model for the upper mantle was prompted by the close match of the south Indian and Canadian shield dispersion curves (Fig. 3). The starting model for inversion thus consisted of a fixed, 35-km-thick crust and a CANSD mantle structure parameterized in terms of 5-km-thick layers extending to a depth of 400 km.

We first inverted the dispersion data by using this starting model. From this we determined two simple-velocity models for the south Indian mantle that fit the data equally well; the first is the simplest model in terms of the number of interfaces and the second is the simplest model in terms of the number of layers. In determining the model with the minimum interfaces, we required the velocity differences between the individual thin layers to be small and the gradients made from the thin layers to be relatively smooth. In determining the model with the minimum number of layers, we examined the early-stage inverted models for adjoining layers that had similar wave speeds and merged these into a single homogeneous layer; this model was used as a starting model in the next inversion stage. We repeated this process until we obtained a satisfactory model whose forward solution matched the significant features of the measured dispersion curves. However, in later inversions the 5-km-thick layer parameterization was reintroduced near the base of the lithosphere to ensure that its depth was not biased by the simplification process used.

The two final models are displayed in Figure 4. The minimum interface upper mantle model (Fig. 4b, black line) consists of a positive shear-wave speed gradient (0.003 sec^{-1}) extending from the base of the crust to about 120 km depth where the maximum shear-wave speed is 4.77 km sec^{-1}. Below this there is a negative wave-speed gradient (0.004 sec^{-1}) extending to about 175 km depth with a LVZ (minimum shear-wave velocity, 4.41 km sec^{-1}) centered at about 200 km depth. The minimum layer upper mantle model (Fig. 4b, gray line; Table 2) consist of a two-layer high-velocity mantle lid of 120-km thickness and average shear-wave speed of 4.68 km sec^{-1}. The two-layer mantle lid corresponds to a shear-wave velocity gradient of about 0.003 sec^{-1}. Below the lid is an 80-km-thick upper mantle LVZ of V_s 4.41 km sec^{-1}, which is underlain by a 92-km-thick layer of V_s 4.68 km sec^{-1} overlying a half-space V_s 5.06 km sec^{-1}. The dispersion curves for both models fit the observed dispersion data equally well (Fig. 4a). Although an infinite number of models might be found that fit the dispersion data alone, the number of models fitting the dispersion data, the crustal structure, and the S_n velocity are more restricted.

Finally, we checked the sensitivity of our dispersion data against the high-velocity lid and LVZ structure of the model. In the first test (Fig. 5) we checked the sensitivity of the dispersion data to the presence of a LVZ beneath a high-velocity upper mantle lid. The high sub-Moho shear-wave velocity is required by the *S*-wave travel time shown in Figure 2 and those previously reported by Huest *et al.* (1973). Removing the LVZ results in the dispersion being overestimated in the 60- to 100-sec period range. Figure 6a,b shows that reducing the sub-Moho shear-wave gradient from 0.003 sec^{-1} to 0.004 sec^{-1} causes the calculated dispersion curve to underestimate the observed dispersion between about a 45- and 60-sec period and to skirt the lower bounds of the observed dispersion at periods longer than 60 sec. Raising the sub-Moho gradient to 0.0015 sec^{-1} causes the calculated dispersion curve to overestimate the observations between about 60 and 90 sec period. Figure 6c,d shows that raising the minimum shear-wave speed in the LVZ to 4.53 km sec^{-1} results in an overestimation of the dispersion in the 60- to 90-sec period range, whereas reducing the minimum shear-wave speed in the LVZ to 4.33 km sec^{-1} results in an underestimate of the dispersion between about a 95- and a 120-sec period. Figure 7a,b shows that increasing the depth to the bottom of the lid of the minimum layer model from 155 km to 175 km overestimates the observed dispersion in the 60- to 90-sec period range, whereas decreasing the base of the lid to 135 km only underestimates the observed dispersion between about a 45- and a 55-sec period. Increasing the depth to the base of the LVZ in the minimum layer model (Fig. 7c,d) from 235 km to 275 km results in an underestimate of the observed dispersion in the 100- to 130-sec period range, while decreasing the depth to the base of the LVZ by a similar amount to 195 km results in an overestimate of the observed dispersion 65- to 95-sec period range.

Table 2
Layer Thickness and Shear-Wave Velocity for the Final Minimum Inversion Model

Layer No.	Thickness (km)	Shear-Wave Velocity (km sec^{-1})
1	20.0	3.489
2	15.0	3.944
3	40.0	4.521
4	80.0	4.765
5	80.0	4.407
6	92.0	4.686
7	∞	5.056

Discussion and Conclusion

The final velocity models for the south Indian shield show a ~155-km-thick seismic lithosphere composed of a 35-km-thick, two-layer crust and a ~120-km-thick, high-velocity upper mantle lid. Beneath the Moho the average S_n wave speed is high, ~4.7 km sec^{-1}. Both S_n travel-times data and the dispersion data suggest a positive sub-Moho shear-wave speed gradient. Beneath the seismic lithosphere there is a low-velocity layer where the shear-wave speed drops to ~4.4 km sec^{-1}. The base of the seismic lithosphere is constrained to $\sim \pm 20$ km, whereas the base of the low-velocity layer is only constrained to $\sim \pm 40$ km. The mantle lid obtained from this study is thicker than that inferred by Bhattacharya (1981) by 15 km, essentially lying within the

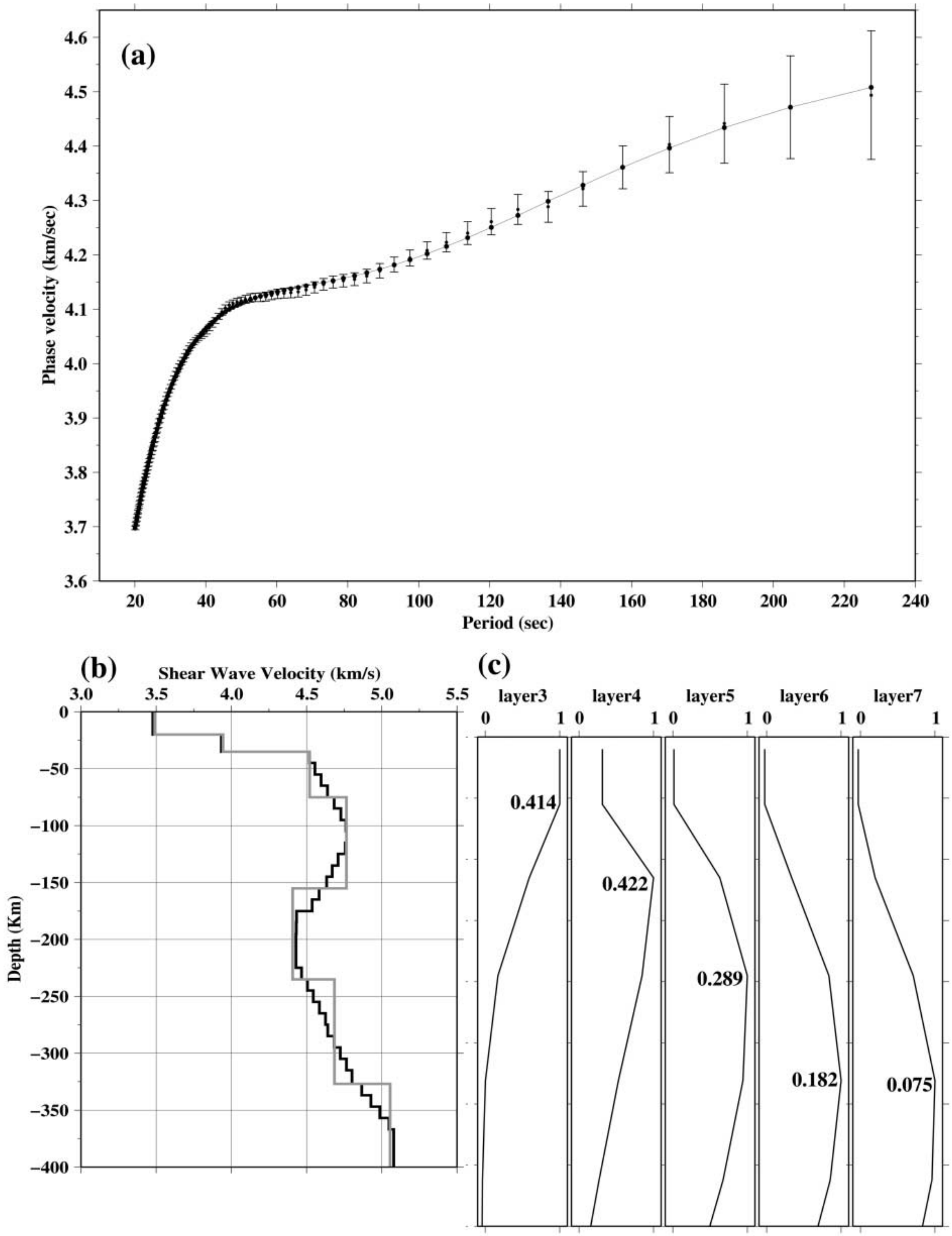

Figure 4. Phase-velocity inversion results for the south Indian shield region. (a) The match of the synthetic dispersion curves with the ±1 S.D. bounds from the data, for the final velocity models. (b) Final velocity models (minimum interface model denoted by the black line; minimum layer model denoted by the gray line). Dispersion curves for both of these models are plotted in (a) and layer and minimum interface velocity models, respectively. Both velocity models fit the dispersion observations equally well. (c) The resolution kernels for the mantle layers in the minimum layer model. All the kernel plots are equalized to one, and the maximum value is given within the individual resolution kernel plots. The layer number corresponding to each resolution kernel is given above the panel showing the resolution kernel.

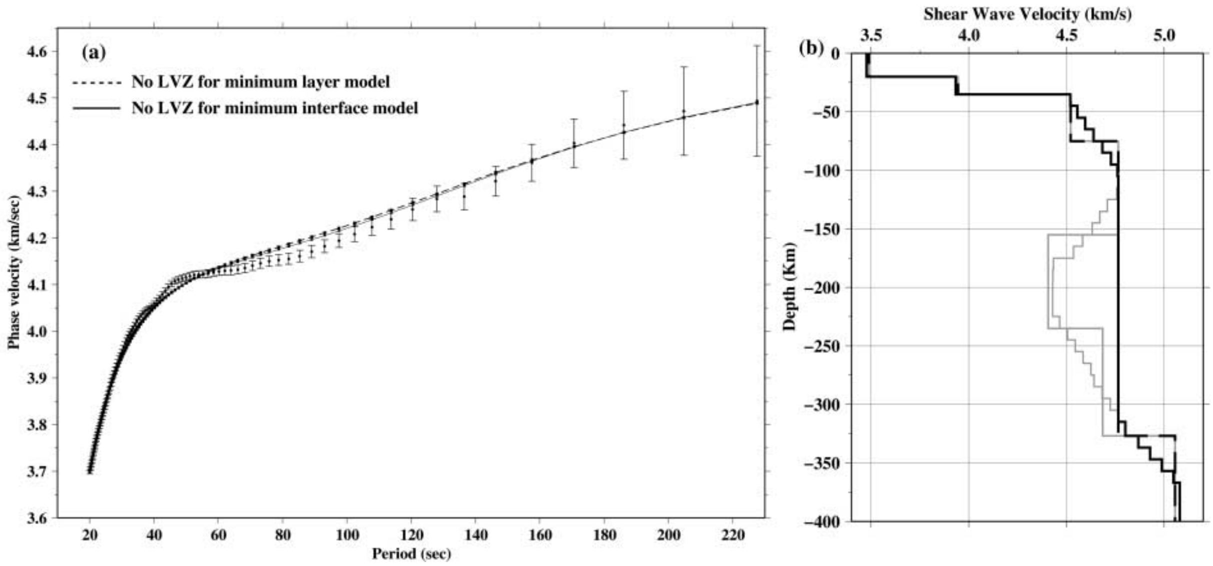

Figure 5. Test of the dispersion data sensitivity to the presence of a low-velocity layer beneath the high-velocity upper mantle lid.

error bounds. Models of the lithosphere inferred by Hwang and Mitchell (1987) for the Indian shield did not contain a LVZ, which most likely resulted from their lack of long-period data. Though the error bounds become larger at longer periods, our inversion models resolve the mantle structures to much greater depths than previous phase-velocity studies in the Indian shield.

Figure 3 compares our fundamental mode Rayleigh wave-phase dispersion curve for peninsular India with dispersion curves from several other major shield regions. The Canadian shield phase-velocity curve (Brune and Dorman, 1963) closely matches the dispersion curve for the south Indian shield to about a 90-sec period, as does the south African, below a 40-sec period. In contrast, the Siberian shield dispersion curve is much slower at all periods. The differences in these dispersion curves from diverse shield regions is attributed to differences in their upper mantle and possibly lower crustal structures. Thus, although the Canadian shield curve closely matches the measured dispersion for the south Indian shield, our final inversion model yielded an 120-km-thick mantle lid, whereas the upper mantle of CANSD is 85 km thick. This may be due to the Canadian shield curve being limited to a 90-sec period (Brune and Dorman, 1963), providing a weaker constraint on the LVZ boundary. The lower velocity for the Siberian shield dispersion curve than for others may be due in part to its thick crust which is 45 km, only a little thicker than the 42 km of south Africa, whose dispersion curve matches the south Indian curve up to 40 sec, but falls below it at lower frequencies. The thicker south African crust compared with India's average of ~35 km apparently shifts its dispersion curve slightly below the south Indian curve, beyond a 40-sec period, but its continuing parallelism to that of India indicates a similar upper mantle structure. This is confirmed by the 160-km-thick lithosphere for the south African shield (Priestley, 1999) similar to our inverted model for the south Indian shield (~155-km-thick lithosphere). The mismatch between the Indian shield dispersion of Hwang and Mitchell (1987) and ours between 20- and 45-sec periods possibly arises from the difference in the average crustal thickness sampled by ray paths of the two data sets. The Hwang and Mitchell (1987) study of an east–west path from Pune to Shillong samples the Western Ghats which is known to have a thicker crust than the average of south India estimated from deep seismic sounding (Kaila and Krishna, 1992), and receiver functions (Rai *et al.*, 2003).

The upper mantle model derived here for the south Indian shield suggests that the Indian cratonic root is somewhat thinner than that found for many other cratons. For example, the cratonic root of the Siberian Platform (Priestley and Debayle, 2003), west Africa (Ritsema and van Heijst, 2000), the European platform (Zielhuis and Nolet, 1994; Priestley and McKenzie, 2006), and North America (Van der Lee and Nolet, 1997; Priestley and McKenzie, 2006) all extend to ~225 km depth or more. On the other hand, there is no seismic evidence for a high-velocity cratonic root beneath the eastern part of the Sino-Korean craton (Priestley and Debayle, 2003; Lebedev and Nolet, 2003), although geologic evidence exists for a cratonic root beneath this region in the Paleozoic (Menzies *et al.*, 1993). Since the late Mesozoic the eastern portion of the Sino-Korean craton has been subjected to rifting and this process has likely attenuated and possibly removed the cratonic root. Perhaps India's rapid translation across the Indian Ocean in the recent geologic past has thinned or attenuated the cratonic root of the south Indian shield.

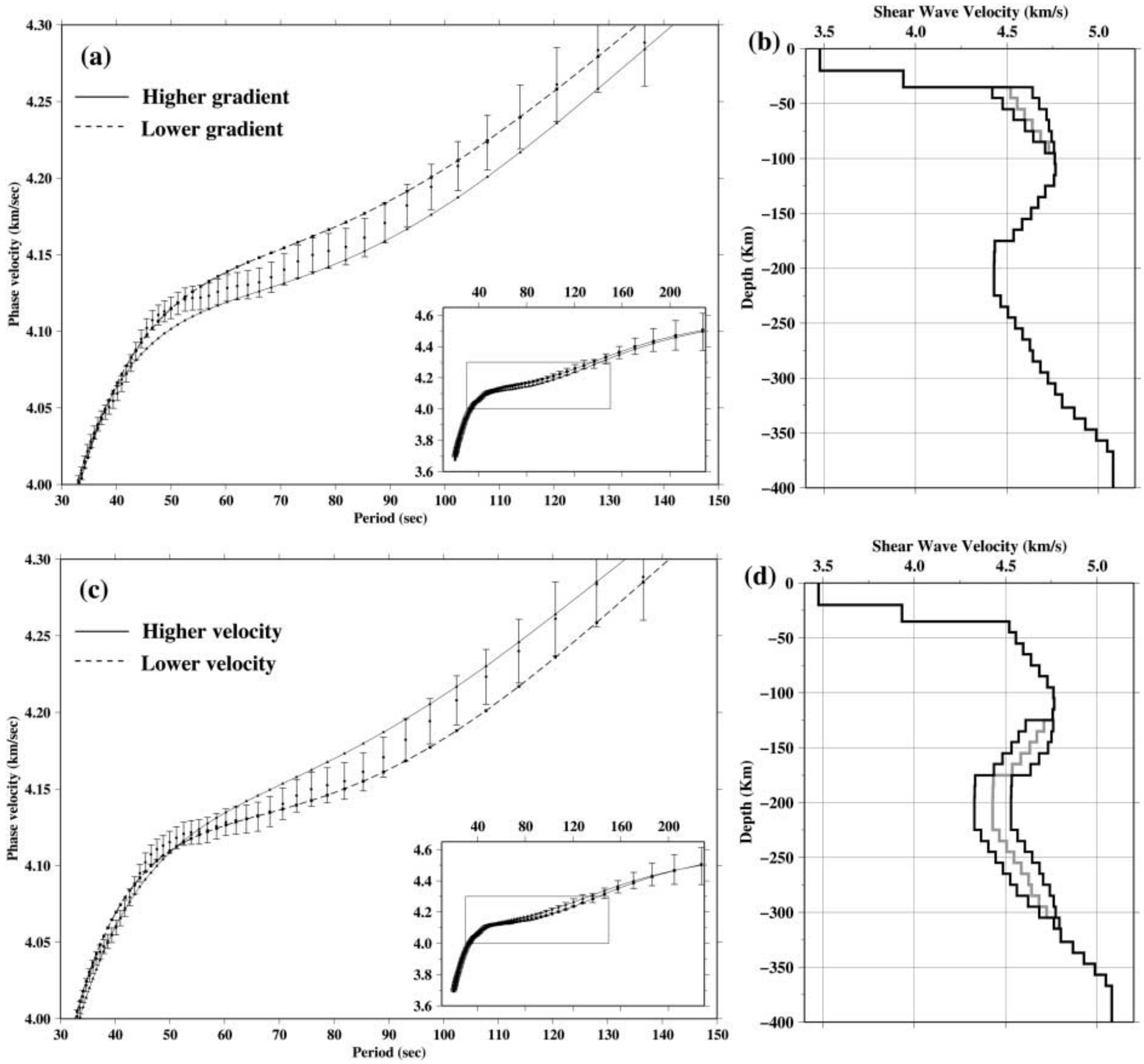

Figure 6. Test of the dispersion data sensitivity to: (a) variation in sub-Moho velocity gradient and (b) $\pm 2.5\%$ perturbation in the minimum velocity of the LVZ.

Acknowledgments

We thank R. B. Hermann for providing the computer programs used in this study. The maps shown in Figures 1 and 2 were made with Generic Mapping Tools. S.M. thanks Cambridge Commonwealth Trust for providing a scholarship to study at the University of Cambridge where this work formed a portion of his Ph.D. research. V.K.G. thanks the Directors of IIA and C-MMACS for providing infrastructure support. The manuscript has benefited from the review and comments of Keith Koper (associate editor) and an anonymous reviewer. This study is Cambridge University Department of Earth Sciences contribution ES8482.

References

Bhattacharya, S. N. (1974). The crust-mantle structure of the Indian Peninsula from surface wave dispersion, *Geophys. J. R. Astr. Soc.* **36,** 273–283.

Bhattacharya, S. N. (1981). Observation and inversion of surface wave group velocities across central India, *Bull. Seism. Soc. Am.* **71,** 1489–1501.

Brune, J. N., and J. Dorman (1963). Seismic waves and earth structure in the Canadian Shield, *Bull. Seism. Soc. Am.* **53,** no. 1, 167–210.

Gomberg, J. S., K. F. Priestley, T. G. Masters, and J. N. Brune (1988). The structure of the crust and upper mantle of northern Mexico, *Geophys. J.* **94,** 1–20.

Gupta, S., S. S. Rai, K. S. Prakasham, D. Srinagesh, B. K. Bansal, R. K. Chadha, K. Priestley, and V. G. Gaur (2003). The nature of South Indian crust: implications for Precambrian crustal evolution, *Geophys. Res. Lett.* **30,** no. 1, 1–4.

Herrmann, R. B. (2004). *Computer Programs in Seismology*, Department of Earth and Atmospheric Sciences, St. Louis University, St. Louis, Missouri.

Huest, S., P. Molnar, and J. Oliver (1973). Regional Sn velocities and shear velocity in the upper mantle, *Bull. Seism. Soc. Am.* **63,** 469–475.

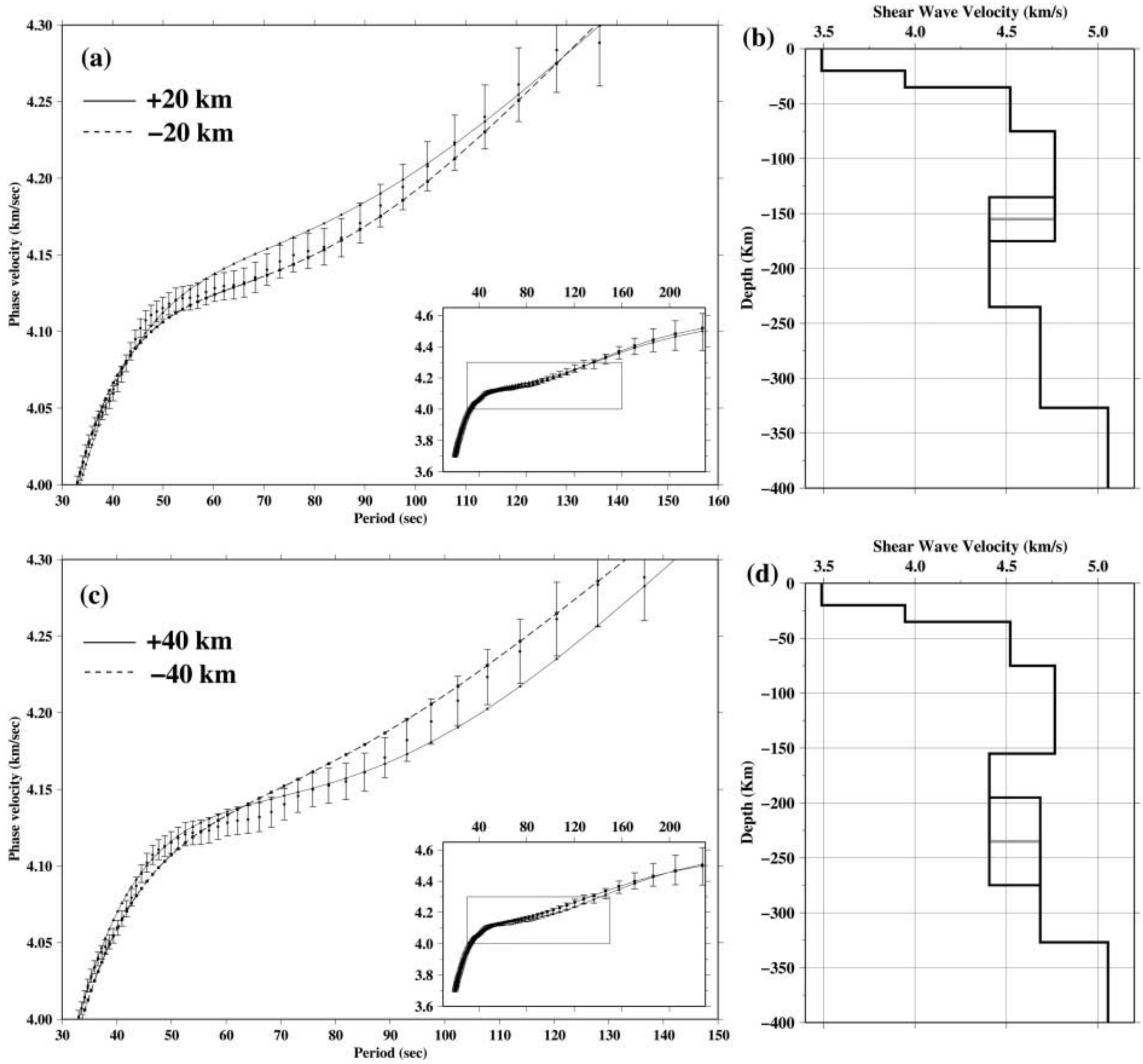

Figure 7. Test of the dispersion data sensitivity to: (a) ±20-km thickness perturbation to the high velocity and (b) ±40 km thickness perturbation to the base of the LVZ layer.

Hwang, H-J., and B. Mitchell (1987). Shear velocities, q_β, and the frequency dependence of q_β in stable and tectonically active regions from surface wave observations, *Geophys. J. Int.* **90,** 575–613.

Kaila, K. L., and V. G. Krishna (1992). Deep seismic sounding studies in India and major discoveries, *Curr. Sci. India* **62,** no. 1-2, 117–154.

Lebedev, S., and G. Nolet (2003). Upper mantle beneath southeast Asia from *S* velocity tomography, *J. Geophys. Res.* **108,** no. B1, doi 10.1029/2000JB000073.

Menzies, M. A., W.-M. Fan, and M. Zhang (1993). Pleozoic and Cenozoic lithosphere and the loss of >120 km of archean lithosphere, Sino-Korean craton, China, in *Magmatic Processes and Plate Tectonics*, H. M. Orichard, H. M. Alabaster, T. Harris, and C. R. Neary (Editors), Geological Society, London, 71–81.

Nataf, H.-C., and Y. Ricard (1996). 3SMAC: an a priori tomographic model of the upper mantle based on geophysical modeling, *Phys. Earth Planet. Interiors* **95,** 101–122.

Priestley, K. (1999). Velocity structure of the continental upper mantle: evidence from southern Africa, *Lithos* **48,** 45–56.

Priestley, K., and E. Debayle (2003). Seismic evidence for a moderately thick lithosphere beneath the Siberian Platform, *Geophy. Res. Lett.* **30,** no. 3, doi 10.1029/2002GL015931.

Priestley, K., and D. McKenzie (2006). The thermal structure of the lithosphere from shear wave velocities, *Earth Planet. Sci. Lett.* **244,** 285–310.

Priestley, K., and F. Tilmann (1999). Shear-wave structure of the lithosphere above the Hawaiian hot spot from two–station Rayleigh wave phase velocity measurements, *Geophy. Res. Lett.* **26,** 1493–1496.

Rai, S. S., K. Priestley, K. Suryaprakasam, D. Srinagesh, V. K. Gaur, and Z. Du (2003). Crustal shear velocity structure of the south Indian shield, *J. Geophys. Res.* **108,** no. B2, doi 10.1029/2002JB001776.

Ritsema, J., and H. J. van Heijst (2000). New seismic model of the upper mantle beneath Africa, *Geology* **28,** 63–66.

Van der Lee, S., and G. Nolet (1997). Upper mantle *S* velocity structure of North America, *J. Geophys. Res.* **102,** 22,815–22,838.

Zielhuis, A., and G. Nolet (1994). Shear wave velocity variations in the upper mantle beneath central Europe, *Geophys. J. Int.* **117,** 695–715.

Bullard Laboratories
University of Cambridge
Cambridge CB3 OEZ, United Kingdom
(S.M., K.P.)

Indian Institute of Astrophysics
Bangalore, India 560 037
(V.K.G.)

Center for Mathematical Modelling and Computer Simulations
Bangalore, India 560 037
(V.K.G.)

National Geophysical Research Institute
Hyderabad, India 500 007
(S.S.R.)

Manuscript received 7 June 2005.